FBXO30 functions as a tumor suppressor and an E3 ubiquitin ligase for hZIP1-mediated HIF-1α degradation in renal cell carcinoma

YULIN YUAN[1], ZIMENG LIU[2], BOHAN LI[1], ZHENG GONG[1], CHIYUAN PIAO[1], ZHUONAN LIU[1], ZHE ZHANG[1] and XIAO DONG[1]

Departments of [1]Urology and [2]Anesthesiology, The First Hospital of China Medical University, Shenyang, Liaoning 110002, P.R. China

Abstract. Studies on clear cell renal cell carcinoma (ccRCC) are gaining momentum due to its high malignancy and potential to metastasize. F-box protein 30 (FBXO30) is a member of the F-box protein family; however, its role and mechanism in cancer remains to be fully elucidated. Western blotting, reverse transcription-quantitative PCR and immunohistochemsitry were performed to detect the expression levels of FBXO30 in ccRCC tissues and adjacent normal tissues. Tumor biological function assays and animal experiments were conducted to clarify the inhibitory effect of FBXO30 on the progression and metastasis of ccRCC. Protein half-life assay, MG132 inhibition assay, immunofluorescence assay and co-immunoprecipitation assay were performed to explore the ubiquitination mechanism of FBXO30 and HIF-1α. Zinc supplementation assay was used to verify the regulatory relationship between human ZRT, IRT-like protein 1 (hZIP1), FBXO30 and HIF-1α. The present study revealed that the expression levels of FBXO30 were lower in ccRCC tissues compared with those in normal adjacent tissues. In addition, FBXO30 inhibited the tumorigenesis and metastatic capacity of ccRCC cells *in vivo* and *in vitro*. FBXO30 mediated the ubiquitination and degradation of hypoxia-inducible factor-1α (HIF-1α) in ccRCC cells under normoxia, thereby inhibiting the oncogenic effect of HIF-1α. Notably, hZIP1 served as an upstream regulator of FBXO30, regulating the expression of FBXO30 and HIF-1α by recruiting Zn^{2+}. In conclusion, the present data suggested that FBXO30 is a novel E3 ubiquitination ligase that can function as a tumor suppressor in ccRCC, and the hZIP1/Zn^{2+}/FBXO30/HIF-1α axis may provide potential biomarkers or therapeutic targets for ccRCC.

Introduction

Renal carcinoma is a commonly diagnosed tumor in the urinary system. In 2022, estimated new cases of kidney cancer ranked 8th among all solid tumors in the United States, with 46,345 and 15,259 expected deaths in China and the United States, respectively (1,2). Clear cell renal cell carcinoma (ccRCC) is the most common pathological subtype and is highly likely to metastasize (3). Patients with distant metastasis often demonstrate unfavorable prognoses even after radical nephrectomy (4).

F-box protein (FBP) 30 (FBXO30) is a member of the FBP family. FBPs participate in the assembly of SKP1-CULLIN1-F-box E3 ubiquitin ligase and act as key substrate-recognition subunits. Based on the different types of substrate-binding domains, FBPs are classified into three groups: FBXs, FBWs and FBLs (5,6). FBXW7 mediates the ubiquitination degradation of c-myc, SOX9, mTOR and cell cycle proteins, thereby enabling tumors to obtain resistance to radiotherapy and chemotherapy (7,8). FBL12 promotes the maturation of undifferentiated thymocytes by targeting aldehyde dehydrogenase 3 for ubiquitination degradation (9). In the FBX protein family, FBXO3 interacts with Smurf1 and degrades it via the ubiquitination pathway, and EP300-interacting inhibitor of differentiation 1 is defined as a direct ubiquitination substrate of FBXO21 (10,11). Despite the fact that the function of FBXO30 was previously unknown, it has recently been indicated that FBXO30 is involved in the intracellular ubiquitination regulation of multiple substrates (12). FBXO30 targets Eg5 for ubiquitinylation, and impairs mitosis and proliferation in the mouse mammary gland (13). FBXO30 has been shown to use stem loop-binding protein as a substrate to regulate chromosome segregation in mouse oocytes (14). In addition, FBXO30 is dysregulated by BMP-Smad signaling and participates in muscle loss (15). In tumors, FBXO30 has been reported to be hypermethylated in prostate cancer and has been identified as a potential clinical biomarker (16,17). In addition, FBXO30 is located near the

Correspondence to: Professor Xiao Dong, Department of Urology, The First Hospital of China Medical University, 155 Nanjing North Street, Shenyang, Liaoning 110002, P.R. China
E-mail: xiao120@hotmail.com

D6S1581 gene and can contribute to genetic susceptibility to nasopharyngeal carcinoma (18). However, the role of FBXO30 in other types of cancer and the specific mechanisms are largely unknown.

Hypoxia-inducible factor-1α (HIF-1α) is universally enriched in solid tumors. Under normoxia, the classical degradation pathway of HIF-1α occurs through the ubiquitin-proteasome pathway after its binding to the Von Hippel-Lindau protein (pVHL) E3 ubiquitin ligase (19). An increasing number of novel E3 ubiquitin ligases using HIF-1α as a specific substrate have been reported in tumors. In breast cancer, Parkin and TNF receptor-associated factor 6 have been shown to target the ubiquitination of HIF-1α. In addition, GSK-3β can mediate the degradation of HIF-1α in hepatoma cells through FBXW7 (20-22). These studies suggested that FBPs may have a role in HIF-1α regulation.

As a member of the ZIP family, the main biological function of human ZRT, IRT-like protein 1 (hZIP1), is to promote the intracellular transport of Zn^{2+} to maintain zinc homeostasis in and out of cells. In prostate cancer tissues, hZIP1 expression is markedly reduced. The decline in intracellular Zn^{2+} levels triggered by the downregulation of hZIP1 abundance may be associated with the tumorigenesis of prostate cancer (23-25). Zn^{2+} is an important microelement that is involved in multiple metabolic processes, such as sugar and lipid metabolism (26). Our previous studies indicated that hZIP1 was downregulated in ccRCC tissues and that it inhibited tumor progression by downregulating HIF-1α (27,28). However, the specific mechanism through which hZIP1 decreases HIF-1α and the role of Zn^{2+} remain unknown.

The present study aimed to verify whether HIF-1α was a novel substrate of FBXO30 in ccRCC cells. In addition, the study aimed to determine whether FBXO30 interacted with HIF-1α and mediated its ubiquitination degradation, and whether hZIP1 downregulated HIF-1α by increasing FBXO30 protein abundance. Finally, to the study explored whether Zn^{2+} served as a crucial intermediary in this process.

Materials and methods

Bioinformatics analyses. UALCAN (http://ualcan.path.uab.edu/) was employed to obtain the expression of FBXO30 in different sample types [533 ccRCC tissues and 72 normal kidney tissues voluntarily donated by patients with ccRCC; The Cancer Genome Atlas (TCGA) dataset: kidney renal cell carcinoma (KIRC)], and to assess the relationship between FBXO30 expression and different pathological grades and clinical stages in patients with ccRCC based on data from TCGA database [dataset (cancer name): KIRC]. The survival curves of patients with ccRCC and with high or low FBXO30 expression levels (TCGA dataset: KIRC) were produced using Gene Expression Profiling Interactive Analysis (http://gepia.cancer-pku.cn/). Patients were split into two groups based on FBXO30 expression: 50% were in the high expression group and 50% were in the low expression group.

Cell culture and transfection. OS-RC-2 and 786-O cells were obtained from The Cell Bank of Type Culture Collection of The Chinese Academy of Sciences and were cultured in RPMI-1640 medium (HyClone; Cytiva) supplemented with 10% fetal bovine serum (FBS; Biological Industries; Sartorius AG). Cells were incubated under normoxia (5% CO_2 and 95% humidity) at 37°C.

The pLVX-Puro-FBXO30 and pLVX-Puro-hZIP1 overexpressing lentiviruses were purchased from Shanghai GeneChem Co., Ltd., and control cells were transfected with empty vectors. Lentivirus packaging was performed using a second generation self-inactivated lentivirus packaging system [GV492 (containing gcGFP, puromycin and the target gene) vector plasmid, 20 μg; pHelper 1.0 vector plasmid, 15 μg; pHelper 2.0 vector plasmid, 10 μg]. Briefly, 293T cells (The Cell Bank of Type Culture Collection of The Chinese Academy of Sciences) were cultured to 50% confluence in a six-well plate with 2 ml culture medium and were transfected with the lentiviruses at a concentration of 10x10⁶ transducing units using HiTransG (Shanghai GeneChem Co., Ltd.) according to the manufacturer's instruction at 37°C for 48 h. After centrifugation at 1,500 x g for 15 min at 4°C, the virus suspension was collected and was then used for transduction. OS-RC-2 and 786-O cells were transduced with virus suspension at 37°C for 48 h (virus volume=cell counts x MOI/virus titer). The multiplicity of infection for OS-RC-2 and 786-O cells was 5. The pGPU6/mCherry/Puro-Negative Control and pGPU6/mCherry/Puro-FBXO30 short hairpin (sh)RNA plasmids were constructed by Shanghai GenePharma Co., Ltd. and cells were transfected using Lipofectamine® 3000 Reagent (Invitrogen; Thermo Fisher Scientific, Inc.) according to the manufacturer's protocol at room temperature for 8 h. After selection with puromycin (2 μg/ml) over 72 h to construct stable cell lines, stable cells transduced with overexpressing lentiviruses and transfected with shRNA plasmids were harvested for subsequent assays; puromycin (1 μg/ml) was used for maintenance of stable cells transduced with overexpressing lentiviruses and transfected with shRNA plasmids. Negative control, FBXO30 and hZIP1 small interfering RNAs (siRNAs) to were purchased from JTSBIO Co. The shRNA and siRNA sequences and the vector transcript numbers are listed in Tables SI and SII.

Patient samples. All ccRCC tissues and corresponding adjacent normal tissues (ANTs; ≥2 cm from the edge of the tumor) were obtained from 64 patients in the Urology Department, The First Hospital of China Medical University (Shenyang, China) between January 2018 and December 2021. The average age of the patients was 54 years (age range, 45-63 years), the sex ratio was 1:1, and all of the patients were diagnosed as ccRCC. A total of 20 pairs of tumor tissues and ANTs were used for western blotting, 24 pairs underwent reverse transcription-quantitative PCR (RT-qPCR) and 20 pairs were used for immunohistochemistry. The groups were classified based on the Fuhrman grade (29); T1 and T2 were defined as low grade, and T3 and T4 were defined as high grade. The present study was approved by the Research Ethics Committee of China Medical University, and the approval number was [2019]2019-65-3; written informed consent was obtained from all patients.

Western blotting. Antibody information is available in Table SIII. All antibodies were used according to the manufacturers' protocols. First, total proteins of OS-RC-2 and

786-O cells were extracted using RIPA solution (RIPA: PMSF, 100:1; cat. no. P0013B; Beyotime Institute of Biotechnology). Protein concentration was determined using Enhanced BCA Protein Assay Kit (cat. no. P0010; Beyotime Institute of Biotechnology). Proteins (40 μg/lane) were then separated by SDS-PAGE on 10% gels. Subsequently, the proteins were transferred onto PVDF membranes, which were blocked with skim milk for 1 h at 37°C. The membranes were then incubated with primary antibodies (1:1,000) overnight at 4°C and with secondary antibodies (1:4,000) for 1 h at 37°C. Finally, the ECL reagents (Beijing Transgen Biotech Co., Ltd.) on a MicroChemi Chemiluminescent Imaging System (DNR Bio-Imaging Systems Ltd.). was used to visualize the blots. Image J 1.6.0 software (National Institutes of Health) was used to determine the ratios of target protein/β-actin.

RNA isolation and RT-qPCR. RNAiso Plus and PrimeScript™ RT Master Mix (both from Takara Biotechnology, Co., Ltd.) were used to isolate total RNA of OS-RC-2 and 786-O cells and synthesize cDNA, respectively, according to the manufacturer's protocols. qPCR was then performed using SYBR® Premix Ex Taq™ (Tli RNaseH Plus) on a LightCycler™ 480II system (Roche Diagnostics). The thermocycling conditions were as follows: initial denaturation at 94°C for 3 min, followed by 45 cycles of denaturation at 95°C for 20 sec, annealing at 55°C for 20 sec and extension at 72°C for 20 sec, and a final extension step at 72°C for 10 min. The $2^{-\Delta\Delta Cq}$ method (30) was performed to calculate the relative expression levels. All of the aforementioned reagents were obtained from Takara Biotechnology, Co., Ltd., unless otherwise specified. Primer sequences are provided in Table SI.

Cell viability assay. OS-RC-2 or 786-O cells ($3x10^3$) were seeded in each well of 96-well plates. After inoculated cells grew to ~$1x10^5$, Cell Counting Kit-8 (CCK-8) working solution (Bimake; CCK-8 total volume, 10:100) was then added to each well. After incubation at 37°C for 1 h, the absorbance of the culture solution was measured at 450 nm using a microplate reader (Model 680; Bio-Rad Laboratories, Inc.) at 24, 48 and 72 h.

5-Ethynyl-2'-deoxyuridine (EdU) assay. An EdU Cell Proliferation Kit (cat. no. C0071S; Beyotime Institute of Biotechnology) was used to assess proliferation. After the cells grew to ~$1x10^5$, EdU reagent (1:1,000) was added to each well and incubated at 37°C for 2 h. Subsequently, cells were successively treated with 4% paraformaldehyde (5 min/time for three times) and 3% Triton X-100 (5 min/time for three times) at room temperature. The cells were then treated with click reaction buffer at 37°C for 30 min, after which Hoechst solution was added for 15 min at room temperature. All reaction steps were performed in the dark. Finally, an immunofluorescence microscope (Olympus Corporation) was used to observe and capture images of the cells.

Wound-healing assay. After cells grew to 100% confluence in 24-well plates, 1-ml pipette tips were used to make a scratch in the center of the wells. The cells were then cultured with serum-free medium at 37°C for 24 h. Cell images were acquired with an inverted microscope (EVOS XL system; cat. no. AMEX12000; Thermo Fisher Scientific, Inc.). ImageJ 1.6.0 software was used to calculate the wound area, as follows: Average scratch width=scratch area/length; cell migration rate=(0 h scratch width-24 h scratch width)/0 h scratch width x100.

Cell migration and invasion assays. Cells were suspended in medium supplemented with 2% FBS ($1x10^5$ cells/well for migration assay and $2x10^5$/well for invasion assay), and 200 μl cell suspension was added to the upper chambers of Transwell plates (pore size, 8.0 μm; Corning, Inc.). In the invasion assay, chambers were covered with Matrigel (Matrigel:serum-free medium, 1:5; 20 μl/chamber; BD Biosciences) for 30 min at 37°C. Subsequently, the chambers were placed into 24-well plates with 600 μl medium (10% FBS) in the lower chamber. After incubation at 37°C for 48 h, the chambers were gently rinsed with PBS and the cells were removed with cotton swabs. Crystal violet solution (cat. no. C0121; Beyotime Institute of Biotechnology) was used for staining (10 min at room temperature). Images were obtained under an inverted light microscope at x100 magnification.

MG132 inhibition and protein half-life assays. For the MG132 (cat. no. HY-13259; MedChemExpress) inhibition assay, cells were treated with MG132 (10 μM/well) after growing to 70-80% confluence in six-well plates for 8 h at 37°C. Subsequently, total protein was extracted and subjected to western blotting as aforementioned to detect the protein expression levels of HIF-1α. For the protein half-life assay, cells were cultured to 80-90% confluence in 100-mm culture dishes and were treated with 10 μM cycloheximide (CHX, cat. no. HY-12320; MedChemExpress) at 37°C. Cells were collected at 0, 20, 40 and 60 min. Subsequently, total protein was extracted and subjected to western blotting as aforementioned to detect the protein expression levels of HIF-1α. The half-life of HIF-1α protein was calculated by scanning the density value of the blots using ImageJ 1.6.0 software.

Immunofluorescence staining assay. Cells were cultured to 80% density in 24-well plates before fixation with 4% paraformaldehyde for 30 min at 37°C. Cells were then incubated with 0.2% Triton X-100 for 30 min at 37°C, followed by blocking with 5% FBS for 30 min at 37°C. Subsequently, the cells were incubated with FBXO30 and HIF-1α antibodies (1:100) at 4°C overnight. Alexa Fluor® 488 and 594 secondary antibodies (cat. nos. ab150077 and ab150080; 1:200; Abcam) were then added and incubated for 60 min in the dark at 37°C. Finally, the cells were treated with DAPI solution [1:3; cat. no. abs9235, Absin (Shanghai) Biotechnology Co., Ltd.] with agitation for 20 min in the dark, and images were captured under a fluorescence microscope.

Co-immunoprecipitation (Co-IP) assay. Cells were lysed in lysis buffer (RIPA:PMSF:proteasome inhibitor, 100:1:1), then the lysate was centrifuged at 13,201 x g for 20 min at 4°C. Appropriate amounts of supernatant were separated for use as input. Subsequently, 2 μg FBXO30, HIF-1α or ubiquitin antibodies and IgG were added to each 500 μl of lysate, with vertical mixing at 4°C overnight. Afterwards, A/G beads (cat. no. B23202; Bimake) were washed with TBS-0.1% Tween (cat.

no. T1081; Beijing Solarbio Science & Technology Co., Ltd.) for 1 h with vertical mixing at 4˚C. Subsequently, 20 μl A/G beads was added to each 500 μl of lysate and vertically mixed at 4˚C for 1 h. Each 20 μl of magnetic beads was isolated using a magnetic separator (cat. no. B23803; Bimake). After being suspended in 10 μl 2X SDS loading buffer (cat. no. P1040; Beijing Solarbio Science & Technology Co., Ltd.), the magnetic beads were incubated at 100˚C for 20 min. Finally, the supernatant was aspirated and subjected to western blotting.

Zinc supplementation assay. Cells were cultured to 70-80% confluence in six-well plates. Subsequently, different concentration of $ZnCl_2$ solution (cat no. 366374; MilliporeSigma) was added to the culture medium for 2 h at 37˚C. Total protein was extracted and subjected to western blotting to detect the protein expression levels of HIF-1α as aforementioned.

Animal experiments. The animal experiments performed in the present study were approved by the Ethics Committee of China Medical University (approval no. KT2022527). A total of 16 SPF/VAF female BALB/c-nude mice (age, ~4 weeks) were obtained from Beijing Vital River Laboratory Animal Technology Co., Ltd. for use in the *in vivo* tumorigenesis experiments and were housed in the Department of Laboratory Animal Science, China Medical University. The nude mice were housed in individual ventilated cages under suitable conditions (temperature, 25˚C; humidity, 55%; ventilation velocity, 0.20 m/sec; light/dark cycle, 12/12 h) and were given free access to sterilized fodder and purified water via feeders on the cages. The nude mice were euthanized through cervical dislocation when they lost 20% of their original body weight. In the tumor transplantation experiment, five mice were included in each group. OS-RC-2 cells ($2x10^6$) transfected with empty or FBXO30 vectors were resuspended in 150 μl serum-free medium with 40% Matrigel and were then injected subcutaneously into the flank of each nude mouse. The tumor mass was recorded after 30 days and tumor volume was recorded every 4 days. In the lung metastasis experiment, each group contained three mice. OS-RC-2 cells ($1x10^6$) transfected with empty or FBXO30 vectors were digested and resuspended in 150 μl sterile PBS, and were then slowly injected into the tail vein of each nude mouse. After ~45 days, the lung tissues were separated and the number of metastatic tumors was counted.

Immunohistochemistry (IHC) assay and hematoxylin and eosin (H&E) staining assay. Moderate-sized (1x1x0.2 cm) fresh ccRCC tissues from human patients were immersed in 4% formalin for 48 h at room temperature, and then dehydrated and embedded in paraffin. The paraffin-embedded tissues were then cut into 4-μm sections. At room temperature, the sections were deparaffinized in xylene I and II for 10 min/time, and were then rehydrated in ethanol gradient solution (from high to low: 100, 95, 80 and 70%, 2 min/time) and washed three times with PBS (3 min/wash). The sections were soaked in sodium citrate antigen retrieval solution (cat. no. C1032; Beijing Solarbio Science & Technology Co., Ltd.) and were put into a microwave for 10 min at 100˚C. An immunohistochemistry kit (cat. no. KIT-9720; Fuzhou Maxim Biotechnology Development Co., Ltd.) was used for immunohistochemistry. The sections were first incubated

with endogenous peroxidase blocker and non-specific dye blocking agent for 10 min at room temperature. The sections were then incubated with FBXO30 antibodies (1:100) at 4˚C overnight, followed by incubation with biotinylated anti-IgG antibody and Streptomyces antibiotic protein-peroxidase (cat. no. KIT-9720; Fuzhou Maxim Biotechnology Development Co., Ltd.) (10 min at room temperature). Sections were stained with a DAB kit for 1 min at room temperature (cat. no. DAB-0031; Fuzhou Maxim Biotechnology Development Co., Ltd.). Finally, sections were observed and images were captured under an inverted light microscope.

For H&E staining, the whole lung tissues from mice were sectioned after paraffin embedding. Subsequently, the sections were dewaxed, rehydrated and stained with 1.0% hematoxylin (cat. no. G4070; Beijing Solarbio Science & Technology Co., Ltd.) for 10 min at room temperature. The samples were then stained with 0.5% eosin (cat. no. G1100; Beijing Solarbio Science & Technology Co., Ltd.) for 2 min at room temperature. Finally, sections were observed, and images were captured under an inverted light microscope.

Statistical analysis. To ensure adequate power, all experiments were performed independently at least three times. All data were statistically analyzed using GraphPad Prism (version 9.0; GraphPad; Dotmatics). The mean values of the groups were compared, and the results were presented as the mean ± standard deviation (SD). Differences between two paired groups were analyzed using the nonparametric paired Student's t-test. Unpaired Student's t-test (two-tailed) was used for differential analysis between groups. One-way ANOVA followed by Dunnett's test was used to analyze the differences between multiple experimental groups and a single control group. Survival analysis was performed using the Kaplan-Meier method and the log-rank test. $P<0.05$ was considered to indicate a statistically significant difference.

Results

FBXO30 is expressed at low levels in ccRCC patients and is associated with poor outcomes. To obtain a preliminary understanding of the relationship between FBXO30 and ccRCC, TCGA database was used to determine the differential expression of FBXO30 in ccRCC tissues and its relevance to the prognosis of patients with ccRCC. The mRNA expression levels of FBXO30 in 533 ccRCC tissues were significantly lower than those in 72 ANTs from the 533 patients with ccRCC (Fig. 1A). The mRNA expression levels of FBXO30 were negatively associated with tumor grade and with the individual cancer stages of ccRCC; the expression levels of FBXO30 decreased with tumor progression and staging (Fig. 1B and C). Furthermore, a prognostic analysis on FBXO30 and RCC was performed using Gene Expression Profiling Interactive Analysis to plot Kaplan-Meier survival curves based on data from TCGA database. The results showed that patients with ccRCC and higher FBXO30 expression were inclined to have better overall survival (Fig. 1D). These data were then validated in clinical specimens acquired from patients with ccRCC. Correspondingly, the results of western blotting demonstrated a significant decrease in the protein expression levels of FBXO30 in ccRCC tissues (Fig. 1E and F). The
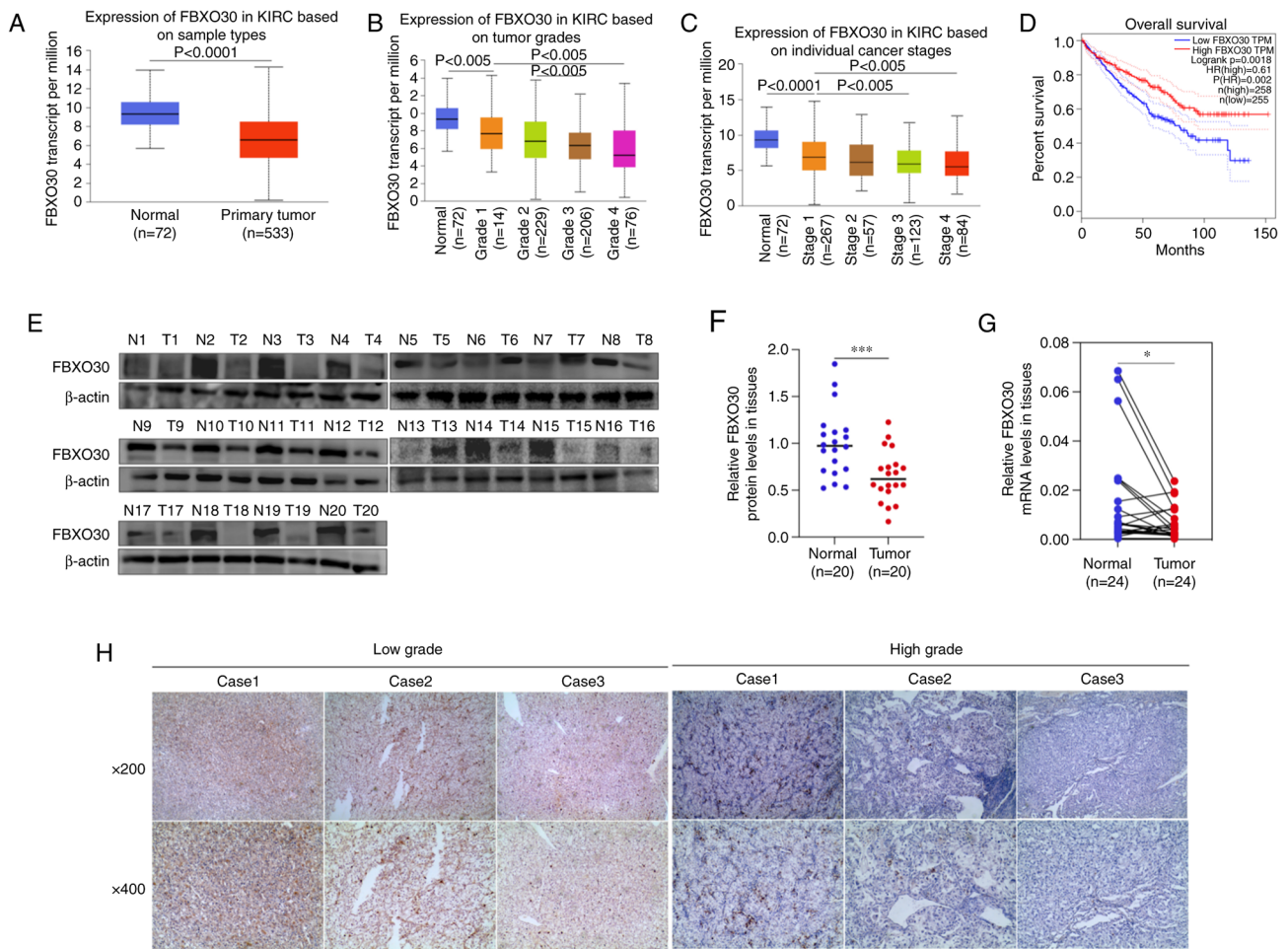
Figure 1. FBXO30 is expressed at low levels in patients with ccRCC and with poor outcomes. (A) FBXO30 expression levels in renal cancer tissues (n=253) and normal tissues (n=72) based on TCGA database. FBXO30 expression levels according to (B) different tumor grades and (C) individual tumor stages in TCGA database. Data were statistically analyzed using one-way ANOVA and Tukey's post hoc test. (D) Kaplan-Meier survival curves depicting overall survival in patients with ccRCC stratified by FBXO30 protein expression based on TCGA database. Cut-off value, 50%. (E and F) Western blotting was employed to detect the protein expression levels of FBXO30 in 20 pairs of clinically derived ccRCC tissues and corresponding ANTs. (G) mRNA expression levels of FBXO30 in 24 pairs of ccRCC tissues and corresponding ANTs, as determined by reverse transcription-quantitative PCR assay. (H) Immunohistochemistry staining of FBXO30 in high-grade and low-grade ccRCC tissues. The high and low groups were classified based on the Fuhrman grade in patients with ccRCC. T1 and T2 were defined as low grade, and T3 and T4 are defined as high grade. Images were acquired with an inverted microscope at x200 and x400 magnification. *P<0.05, ***P<0.001, as determined by paired Student's t-test. ANTs, adjacent normal tissues; ccRCC, clear cell renal cell carcinoma; FBXO30, F-box protein 30; KIRC, kidney renal clear cell carcinoma; N, normal; T, tumor; TCGA, The Cancer Genome Atlas.

mRNA expression levels of FBXO30 were also downregulated in ccRCC tissues, as determined by RT-qPCR (Fig. 1G). In addition, IHC results further revealed that FBXO30 exhibited deeper staining in low-grade ccRCC tissues, indicating that FBXO30 protein expression was negatively associated with the progression of ccRCC (Fig. 1H).

FBXO30 disruption fosters malignant behaviors in ccRCC cells. To explore the biological function of FBXO30 in ccRCC, FBXO30 was stably knocked down in OS-RC-2 and 786-O cells and the knockdown efficiency was confirmed by western blotting (Fig. 2A). CCK-8 and EdU assays were then performed to measure the proliferation of cells. As determined using the CCK-8 assay, knockdown of FBXO30 significantly enhanced the proliferation of OS-RC-2 and 786-O cells (Fig. 2B). As determined using the EdU assay, enhanced EdU fluorescent signals were observed in FBXO30-knockdown ccRCC cells, which suggested that the ccRCC cells had a stronger proliferative capacity after FBXO30 knockdown (Fig. 2C). In the

wound-healing assay, FBXO30 knockdown increased the wound-healing area in the center of the scratch, indicating that FBXO30 knockdown promoted the migration of ccRCC cells (Fig. 2D). Consistently, in the Transwell assay, ccRCC cells with FBXO30 knockdown more easily passed through the membrane in the Transwell chamber, as more stained cells were observed (Fig. 2E). Furthermore, to detect the change in the invasive ability of cells, Matrigel was used to coat the Transwell chamber to simulate the extracellular matrix *in vivo*. It was revealed that more cells passed through the Matrigel and membrane in the FBXO30-knockdown group, and silencing FBXO30 significantly augmented the invasiveness of OS-RC-2 and 786-O cells (Fig. 2E). Finally, western blotting was performed to evaluate epithelial-mesenchymal transition (EMT)-related proteins and it was revealed that knockdown of FBXO30 upregulated N-cadherin and vimentin expression, but downregulated E-cadherin expression, which indicated that FBXO30 knockdown contributed to the EMT process in ccRCC cells (Fig. 2F). These results suggested that inhibition
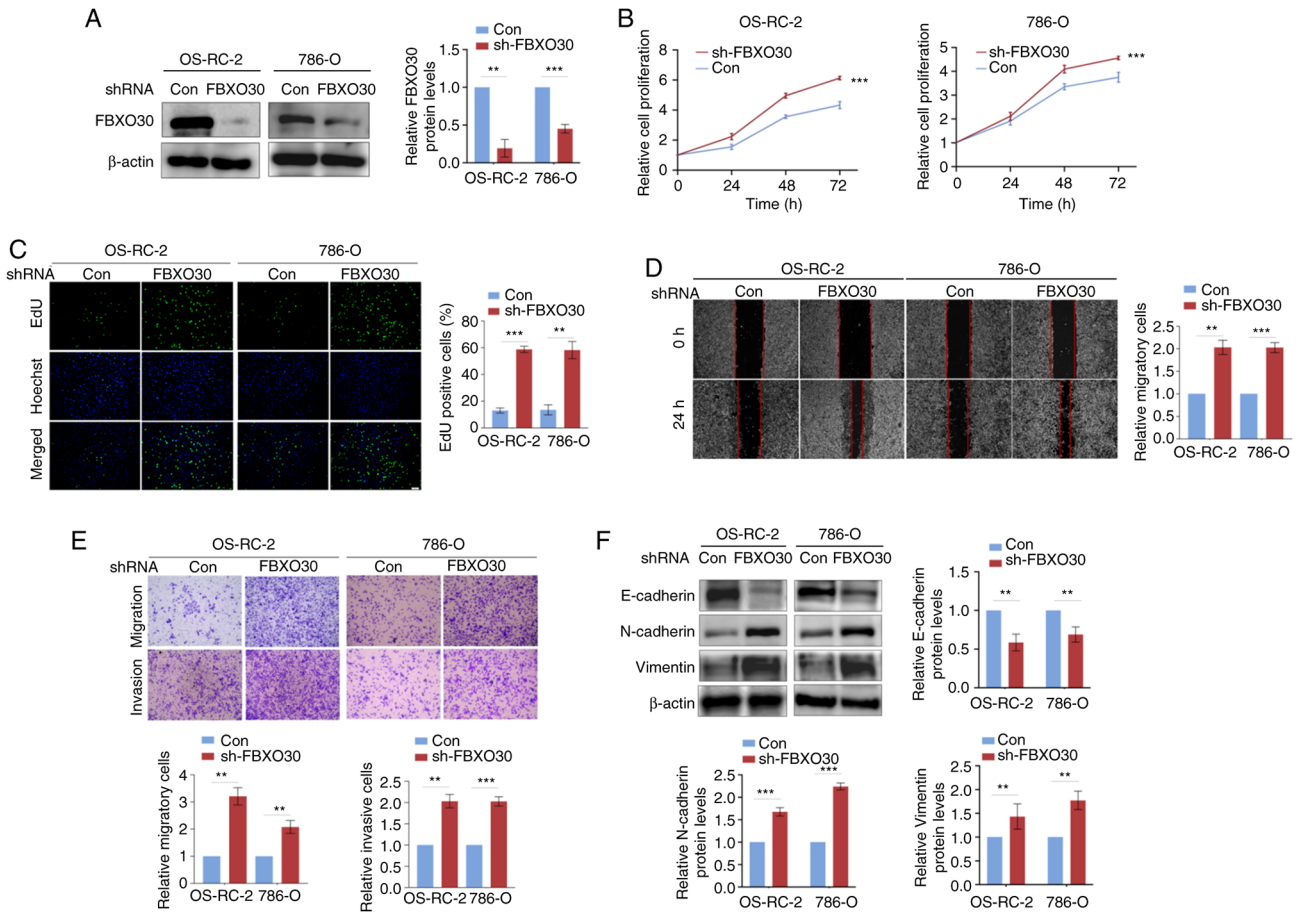
Figure 2. FBXO30 knockdown enhances proliferation, migration and invasion in ccRCC cells. (A) Knockdown efficiency of FBXO30 in OS-RC-2 and 786-O cells was detected by western blotting. (B) Cell viability was measured using the Cell Counting Kit 8 in FBXO30-knockdown OS-RC-2 and 786-O cells. (C) An EdU assay was performed to evaluate the proliferative capacity of cells. Immunofluorescence microscopy (x100 magnification) was used to capture images. Cell migration and invasion were measured using (D) wound-healing and (E) Transwell assays in FBXO30-knockdown OS-RC-2 and 786-O cells. Images were captured under an inverted microscope (x100 magnification). (F) Expression levels of epithelial-mesenchymal transition-related proteins in OS-RC-2 and 786-O cells with FBXO30 knockdown. **P<0.01 and ***P<0.001, as determined by unpaired Student's t-test (two-tailed). EdU, 5-ethynyl-2'-deoxyuridine; FBXO30, F-box protein 30; shRNA, short hairpin RNA.

of FBXO30 could promote the proliferation, migration, invasion and EMT progression of ccRCC cells.

FBXO30 suppresses malignant behaviors in ccRCC cells. The present study also constructed FBXO30-overexpressing OS-RC-2 and 786-O cells, and the overexpression efficiency was confirmed by western blotting (Fig. 3A). Notably, FBXO30 overexpression limited the viability and proliferative capacity of two ccRCC cell lines, as determined by the CCK-8 and EdU assays (Fig. 3B and C). Furthermore, FBXO30 overexpression significantly reduced the migratory capacity of ccRCC cells in both the wound-healing and Transwell migration assays (Fig. 3D and E). FBXO30 overexpression also suppressed the invasiveness of OS-RC-2 and 786-O cells in the Transwell invasion assay (Fig. 3E). Furthermore, FBXO30 inhibited the EMT process, upregulating E-cadherin expression, but downregulating N-cadherin and vimentin expression in ccRCC cells (Fig. 3E and F). These data further verified that FBXO30 might function as a tumor suppressor gene in ccRCC.

FBXO30 mediates the ubiquitination and degradation of HIF-1α in ccRCC cells. To study the relationship between

FBXO30 and HIF-1α, FBXO30 was first knocked down in the OS-RC-2 and 786-O cell lines using siRNA and the transfection efficiency was tested by western blotting. It was revealed that the protein expression levels of HIF-1α increased (Fig. 4A). Conversely, overexpression of FBXO30 in these cell lines decreased the expression levels of the HIF-1α protein (Fig. 4A and B). However, there were no significant alterations in the mRNA expression levels of HIF-1α in RCC cells with both knockdown and overexpression of FBXO30 (Fig. 4C and D). These results indicated that FBXO30 tended to post-translationally regulate HIF-1α.

FBXO30-overexpressing OS-RC-2 cells were subsequently treated with the proteasome inhibitor MG132. There was a significant difference in HIF-1α protein expression levels before and after treating FBXO30-overexpressing OS-RC-2 cells with MG132. It was revealed that MG132 could reverse the negative regulation of HIF-1α by FBXO30 (Fig. 4E), indicating that the downregulation of HIF-1α mediated by FBXO30 was, at any rate, partially dependent on the proteasomal degradation pathway. Therefore, the protein synthesis inhibitor CHX was used to test the effect of FBXO30 on the degradation of HIF-1α. Notably, FBXO30 prominently shortened the half-life of HIF-1α protein (Fig. 4F).
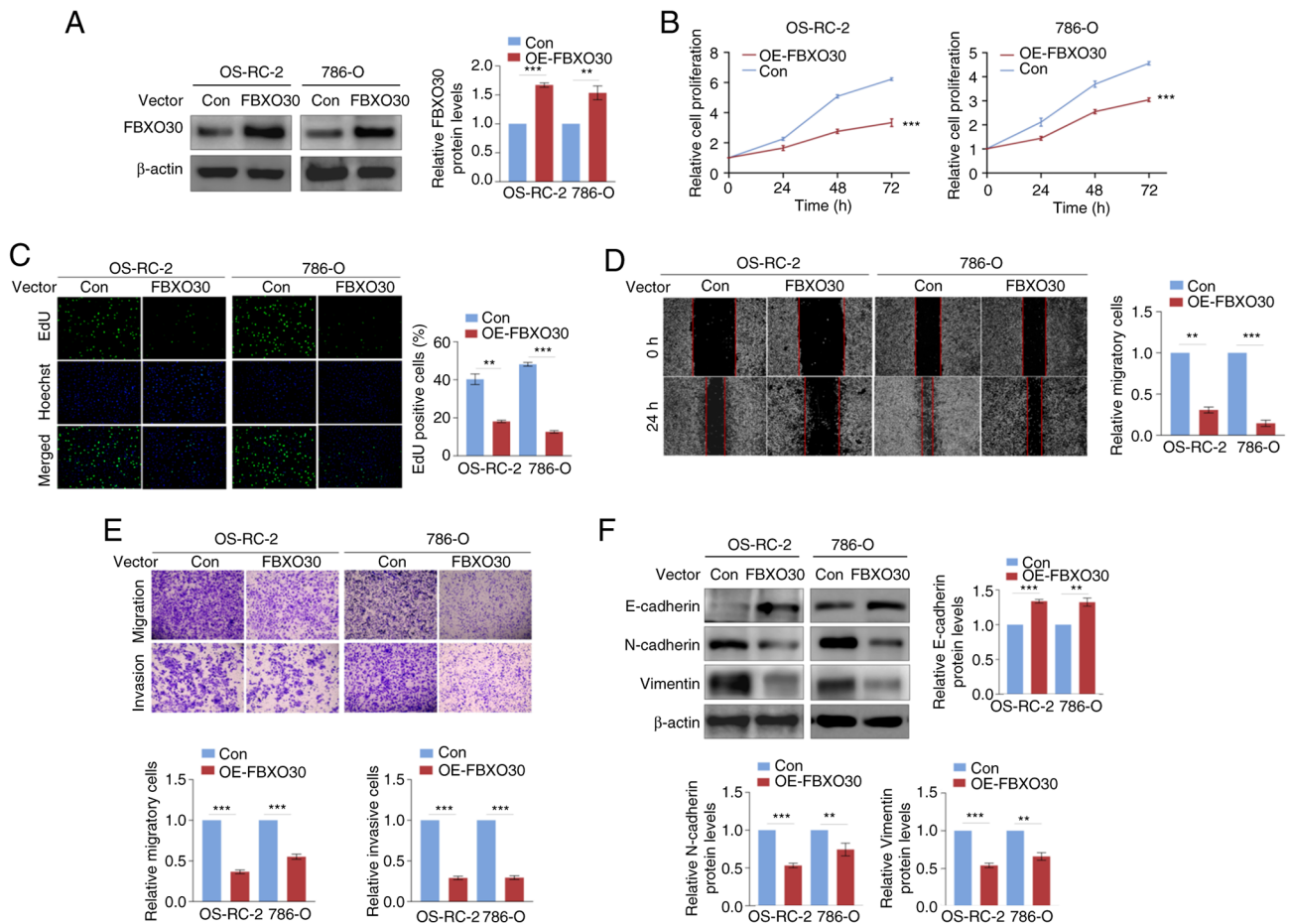
Figure 3. FBXO30 suppresses the proliferation, migration and invasion of ccRCC cells. (A) OE efficiency of FBXO30 in OS-RC-2 and 786-O cells, as measured by western blotting. (B) Cell viability was evaluated using the Cell Counting Kit 8 in FBXO30-overexpressing OS-RC-2 and 786-O cells. (C) An EdU assay was performed to detect the proliferative capacity of cells. Immunofluorescence microscopy (x100 magnification) was used to capture images. Cell migration and invasion were measured using (D) wound-healing and (E) Transwell assays in FBXO30-OE OS-RC-2 and 786-O cells. Images were captured under an inverted microscope (x100 magnification). (F) Expression levels of epithelial-mesenchymal transition-related proteins in OS-RC-2 and 786-O cells overexpressing FBXO30. **P<0.01 and ***P<0.001, as determined by unpaired Student's t-test (two-tailed). EdU, 5-ethynyl-2'-deoxyuridine; FBXO30, F-box protein 30; OE, overexpression.

Considering that FBXO30 may act as an E3 ubiquitin ligase because it belongs to the FBP family, it was hypothesized that FBXO30 was able to regulate the protein levels of HIF-1α through the ubiquitin-proteasome degradation pathway. The results of the immunofluorescence colocalization assay preliminarily showed that the localization of FBXO30 and HIF-1α in OS-RC-2 cells almost coincided, with these two proteins more likely to be located in the nucleus (Fig. 4G). Furthermore, co-IP experiments showed that FBXO30 directly bound to HIF-1α in OS-RC-2 and 786-O cells (Fig. 4H). Notably, overexpression of FBXO30 facilitated the conjugation of ubiquitin to HIF-1α in coIP assay (anti-ubiquitin) (Fig. 4I). Taken together, these data suggested that in ccRCC cells, FBXO30 was highly likely to downregulate the protein expression levels, but not the mRNA expression levels of HIF-1α through the ubiquitin proteasome pathway.

hZIP1 regulates HIF-1α and FBXO30 in a Zn^{2+}-dependent manner in ccRCC cells. Given that our previous study reported that hZIP1 downregulated HIF-1α expression (25), the present study aimed to determine whether FBXO30 had a role in this process. Thus, the present study examined the expression levels of FBXO30 in hZIP1-overexpressing OS-RC-2 and 786-O cells. The hZIP-1 overexpression efficiency was tested by western blotting. Notably, overexpression of hZIP1 increased the protein expression levels of FBXO30 in OS-RC-2 and 786-O renal cancer cells (Fig. 5A). Furthermore, knockdown of FBXO30 rescued the downregulation of HIF-1α protein expression levels induced by hZIP1 to some extent (Fig. 5A and B), which verified the hypothesis that hZIP1 decreased HIF-1α protein expression levels at least partially by downregulating FBXO30 expression.

It has previously been reported that hZIP1 serves as a transport protein to transfer Zn^{2+} from the extracellular zone to the intracellular area (22). To explore the potential function of Zn^{2+}, RCC cells were treated with progressively increasing concentrations of $ZnCl_2$. It was revealed that the protein expression levels of HIF-1α were negatively associated with the concentration of Zn^{2+}, and the optimal inhibiting concentration was likely to be ~20 μM (Fig. 5C). Correspondingly, treatment with 20 μM Zn^{2+} resulted in upregulation of FBXO30 protein expression levels in OS-RC-2 and 786-O cells (Fig. 5D). To ultimately identify the role of Zn^{2+}, hZIP1-knockdown RCC cells were treated
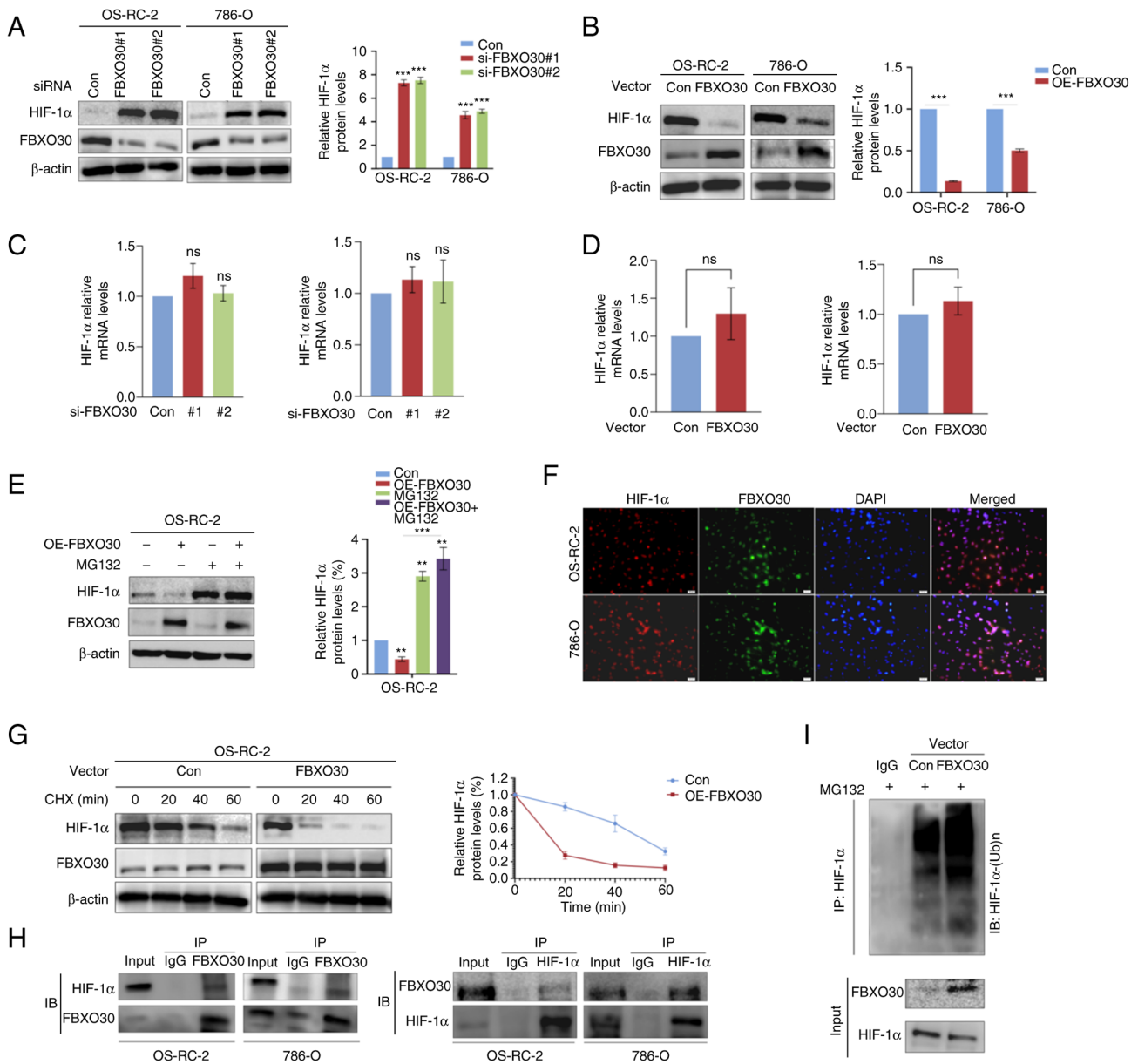
Figure 4. FBXO30 mediates the ubiquitination and degradation of HIF-1α in ccRCC cells. After (A) knockdown and (B) OE of FBXO30 in OS-RC-2 and 786-O cells, HIF-1α protein expression was detected, and the efficiency of knockdown and overexpression was examined by western blotting. Reverse transcription-quantitative PCR was performed to detect the mRNA expression levels of HIF-1α in (C) FBXO30-knockdown and (D) FBXO30-OE OS-RC-2 and 786-O cells. (E) Western blotting was performed to determine the effect of the proteasome inhibitor MG132 (10 μM, 8 h) on HIF-1α protein expression in OS-RC-2 cells, and MG132 rescued the downregulation of HIF-1α in FBXO30-overexpressing OS-RC-2 cells. (F) FBXO30 OE reduced the half-life of HIF-1α protein. Under normoxia, OS-RC-2 cells were treated with CHX (10 μM) at preset time points. Subsequently, the cells were harvested and subjected to western blotting. (G) Immunofluorescence colocalization assay demonstrated that in OS-RC-2 and 786-O cells, HIF-1α (red) possessed the same subcellular localization as FBXO30 (green), almost coinciding with nuclear staining (blue). Images were captured under an immunofluorescence microscope (x200 magnification). (H) Co-IP assay indicated endogenous binding between FBXO30 and HIF-1α in both OS-RC-2 and 786-O cells. (I) FBXO30 promoted the conjugation of ubiquitin to HIF-1α in OS-RC-2 cells and targeted HIF-1α for degradation. **P<0.01 and ***P<0.001 as indicated or vs. control; ns, not significant. Data were analyzed by (A, C and E) one-way ANOVA and Tukey's post hoc test, or (B and D) unpaired Student's t-test. CHX, cycloheximide; FBXO30, F-box protein 30; HIF-1α, hypoxia-inducible factor-1α; IB, immunoblot; IP, immunoprecipitation; OE, overexpression; siRNA, small interfering RNA.

with 20 μM Zn^{2+}. Notably, Zn^{2+} rescued the expression of FBXO30 and reduced the protein expression levels of HIF-1α after treating hZIP1-knockdown OS-RC-2 and 786-O cells with ZnCl$_2$, which suggested that hZIP1 may regulate the protein expression levels of FBXO30 and HIF-1α by altering the concentration of Zn^{2+} in ccRCC cells (Fig. 5E).

To preliminarily understand the possible effects of zinc ions on glycolysis in ccRCC cells, the expression levels of some enzymes in glycolysis were detected, namely, pyruvate dehydrogenase kinase 1 (PDK1), lactate dehydrogenase A (LDHA) and glucose transporter 1 (GLUT1), which were proven to be regulated by HIF-1α (31). The present study revealed that Zn^{2+} significantly downregulated the expression levels of PDK1, LDHA and GLUT1 (Fig. 5F). Overall, hZIP1 downregulated HIF-1α through FBXO30, in which Zn^{2+} exerted an essential intermediary role.

FBXO30 inhibits tumor growth in vivo. To further verify the tumor biological function of FBXO30 *in vivo*, OS-RC-2 cells
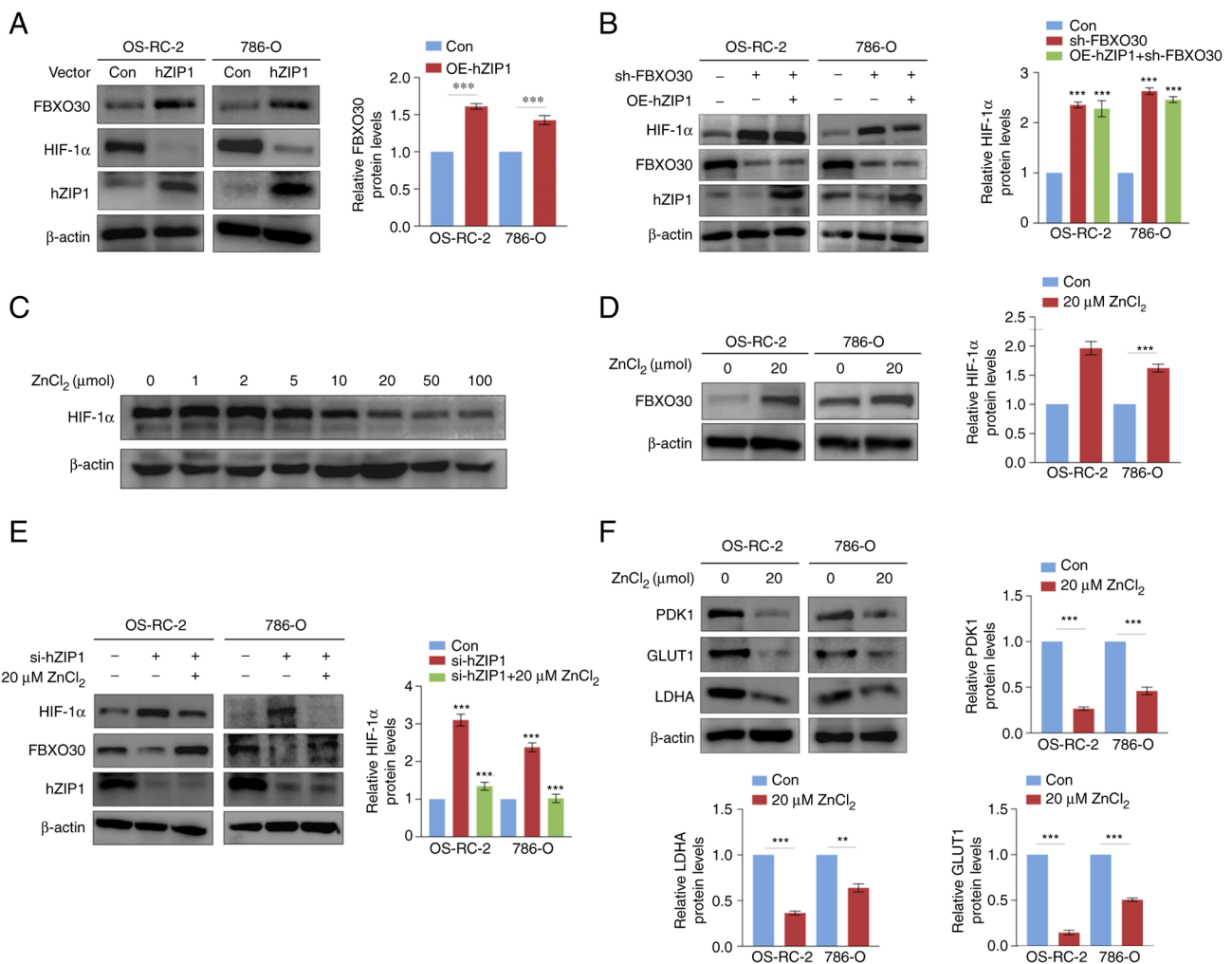
Figure 5. hZIP1 regulates HIF-1α and FBXO30 in a Zn^{2+}-dependent manner in ccRCC cells. (A) OE of hZIP1 in OS-RC-2 and 786-O cells inhibits the expression of HIF-1α and upregulates the protein expression levels of FBXO30. (B) Western blotting demonstrated that FBXO30 knockdown rescued HIF-1α depletion in hZIP1-OE OS-RC-2 and 786-O cells. (C) Zinc supplementation assay confirmed that zinc ions inhibited the expression of HIF-1α in OS-RC-2 cells, and 20 μM was defined as the optimal inhibitory concentration. After the addition of increasing concentrations of $ZnCl_2$ solution to the culture medium for 2 h at 37°C in normoxia, the cells were collected and lysed for western blotting. (D) Upregulation of FBXO30 was induced by optimal concentrations of zinc ions in OS-RC-2 and 786-O cells. (E) FBXO30 downregulation and HIF-1α accumulation were observed after knockdown of hZIP1, whereas supplementation with zinc ions counteracted this alteration in the expression levels of FBXO30 and HIF-1α in hZIP1-knockdown OS-RC-2 and 786-O cells. ***P<0.001 in (B and E) was obtained by comparing each experimental group with control group. (F) Zinc ions downregulated the expression levels of glucose metabolism-related enzymes (PDK1, GLUT1 and LDHA). **P<0.01 and ***P<0.001 as indicated or vs. control. Data were analyzed by (B and E) one-way ANOVA and Dunnett's post hoc test, or (A, D and F) unpaired Student's t-test. FBXO30, F-box protein 30; GLUT1, glucose transporter 1; HIF-1α, hypoxia-inducible factor-1α; hZIP1, human ZRT, IRT-like protein 1; LDHA, lactate dehydrogenase A; OE, overexpression; PDK1, pyruvate dehydrogenase kinase 1; sh, short hairpin.

transfected with the empty and FBXO30 vectors were subcutaneously injected into the flank of nude mice. After 30 days, the nude mice were euthanized, and the tumors were excised and weighed. FBXO30 overexpression markedly inhibited tumor formation, as evidenced by the lower tumor weight (Fig. 6A and B).

Subsequently, a lung metastasis model was established in nude mice to evaluate the effect of FBXO30 on tumor metastasis *in vivo*. Lung metastasis models using immune-deficient mice can be used to effectively evaluate the level of tumor invasion and metastasis, and are universally applied in the construction of RCC cell tumor models with a high success rate (32). ccRCC cells transfected with the empty and FBXO30 vectors were injected via the tail vein into nude mice, and the lung tissues were isolated after 45 days. There were approximately six tumor metastases in the lung tissues from the

control group, but only two in the FBXO30 overexpression group. This result indicated that FBXO30 markedly restricted the formation of lung metastases. Subsequently, lung tissues from the two groups were sectioned and subjected to H&E staining. The number of tumor metastatic nodules per field of view was four in the control group and one in the FBXO30 overexpression group. The number of lung metastatic nodules following FBXO30 overexpression was markedly reduced, suggesting that FBXO30 inhibited the metastatic capacity of ccRCC cells *in vivo* (Fig. 6C). Finally, the subcutaneous tumors of nude mice were lysed and proteins were extracted for western blotting. It was revealed that in the subcutaneous tumor tissue from the FBXO30 overexpression group, the expression levels of HIF-1α and proliferating cell nuclear antigen were significantly decreased (Fig. 6D). These results indicated that FBXO30 significantly reduced the accumulation
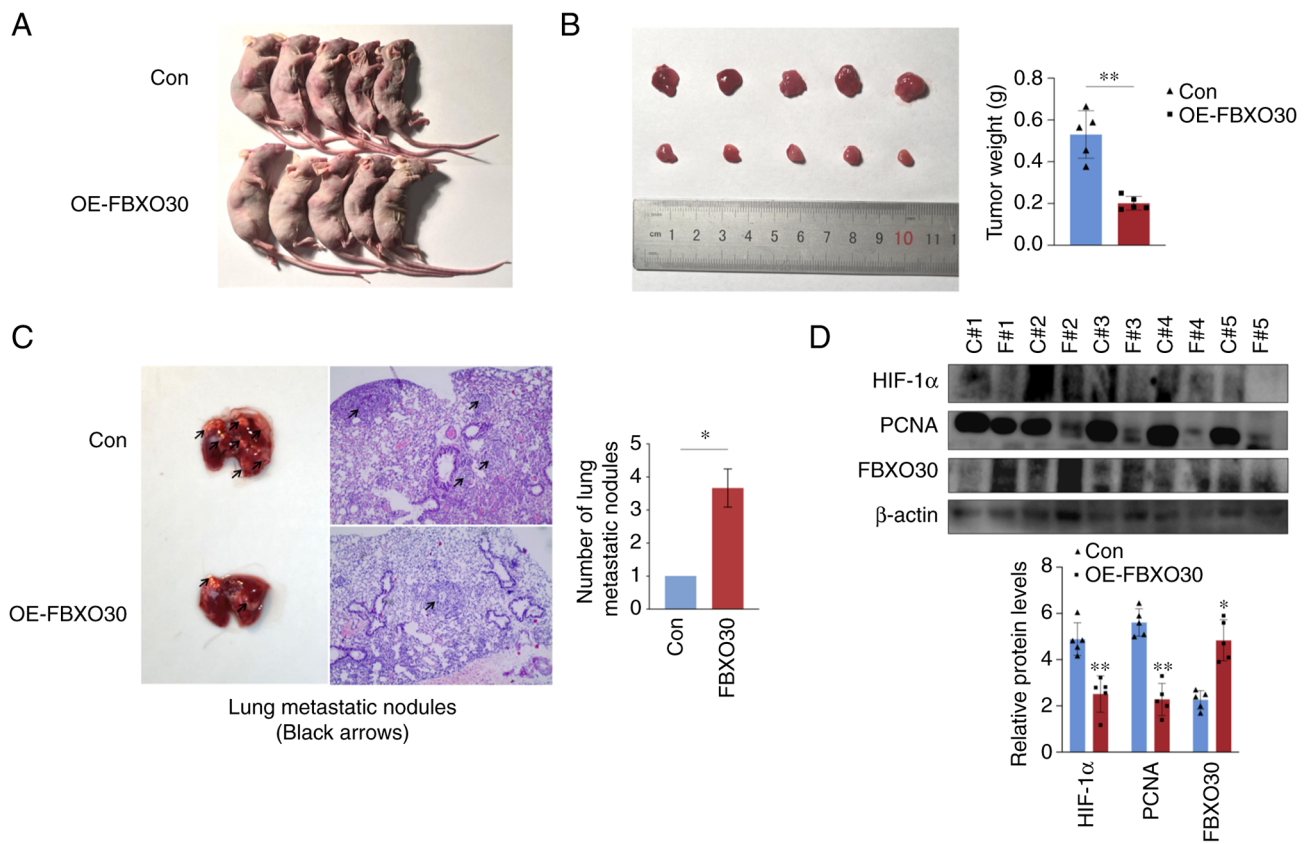
Figure 6. FBXO30 inhibits tumor growth *in vivo*. (A) Representative images of BALB/c nude mice 30 days after subcutaneous inoculation of OS-RC-2 cells transfected with empty vector and FBXO30 vector. (B) Representative images of tumors separated from the nude mice. (C) Representative images of the lungs with tumor metastases excised from nude mice, which were then subjected to hematoxylin and eosin staining. The numbers of metastatic nodules were counted, with three lung metastasis sections contained in each group. Images were captured under an inverted microscope (x100 magnification). (D) Western blotting was performed to detect the protein expression levels of HIF-1α, PCNA and FBXO30. C#, Con; F#, OE-FBXO30. *P<0.05, **P<0.01, as determined by unpaired Student's t-test (two-tailed). FBXO30, F-box protein 30; HIF-1α, hypoxia-inducible factor-1α; OE, overexpression; PCNA, proliferating cell nuclear antigen.

of HIF-1α in tumors *in vivo* and decreased tumor proliferative activity. These data suggested that FBXO30 could inhibit the tumorigenic and metastatic capacity of ccRCC cells *in vivo*.

Discussion

ccRCC is a solid tumor characterized by hypoxia, which is possibly caused by long-term elevated oxygen consumption and decreased oxygen diffusion due to the irregular distribution of the vasculature system in tumors (33-35). However, our previous studies confirmed that even without oxygen content changes in the tumor extracellular microenvironment, HIF-1α, which is supposed to be degraded via pVHL-mediated ubiquitination, remained highly expressed in cultured ccRCC cell lines under normoxia (8,28). Consistently, previous studies have suggested that pVHL is frequently mutated and inactivated during the development of ccRCC (19,33). Therefore, it is still valuable to determine the potential regulatory mechanism of HIF-1α in ccRCC cells with a sufficient oxygen supply. The present study proposed that FBXO30, as a novel E3 ubiquitin ligase, could promote HIF-1α degradation through the ubiquitin-proteasome pathway in normoxia and directly inhibit ccRCC tumor progression.

As a member of the FBP family, the role of FBXO30 in ccRCC remains unclear. FBXO30 has been reported to

target intracellular ubiquitination to regulate cell mitosis and to control muscle growth through the BMP signaling pathway (12,14,15). In cancer, FBXO30 has been reported to be associated with the occurrence of prostate cancer and nasopharyngeal cancer (16,17). In the present study, FBXO30 expression was lower in ccRCC tissues than in ANTs, at both the mRNA and protein levels. IHC assays also suggested that FBXO30 was negatively associated with the malignancy of ccRCC. These results were in accordance with data from TCGA database. Subsequently, it was revealed that FBXO30 suppressed EMT progression in ccRCC *in vitro*. HIF-1α is thought to enhance the invasiveness of ccRCC cells by promoting glycolysis and preventing tumor cells from undergoing apoptosis (36-38). Based on our previous results, HIF-1α has also been reported to act as an oncogene in ccRCC (28). In the present study, FBXO30 reduced the upregulation of HIF-1α protein expression in ccRCC cells under normoxia without affecting its mRNA levels, which could be due to post-translational regulation. FBXO30 possesses the potential to be classed as a novel ubiquitin ligase (5,39). It is reasonable to hypothesize that FBXO30 may act as a possible E3 ubiquitin ligase of HIF-1α. HIF-1α has been reported to enhance EMT progression in peritoneal epithelial cells by increasing the expression levels of VEGF, Snail-1 and MMP-2 proteins (40). In lung cancer,

HIF-1α has been shown to increase the abundance of angiopoietin-like 4 to promote tumor metastasis (41). In addition, HIF-1α can upregulate lysyl oxidase expression in hepatoma cells, inducing cancer metastasis and development (42). Collectively, FBXO30 was able to reduce HIF-1α upregulation in ccRCC cells through the ubiquitin-proteasome degradation pathway, thus inhibiting tumor progression and metastasis.

Consistently with our previous study, FBXO30 was knocked down in hZIP1-overexpressing ccRCC cells, and the depletion of FBXO30 rescued HIF-1α downregulation triggered by hZIP1. Given that hZIP1 is a known Zn^{2+} transport protein, the function of Zn^{2+} was investigated. Zinc is involved in immune system defense, and is associated with the development of inflammation, metabolism and cancer (43). Zinc has been proven to restrict the malignancy of prostate cancer cells (44). In addition, colorectal cancer and adrenal cancer have been shown to be accompanied by zinc deficiency, and Zn^{2+} also demonstrates cytotoxicity to cancer cells (45). In ccRCC, low-concentration Zn^{2+} treatment was capable of effectively inhibiting cancer progression (46). In the present study, the protein expression levels of HIF-1α were decreased in ccRCC cells with increasing Zn^{2+} concentrations. Coincidentally, the findings of Nardinocchi et al (47) showed that zinc also suppressed the expression of HIF-1α and VEGF in prostate cancer and glioblastoma. Notably, zinc supplementation rescued the decrease in FBXO30 and HIF-1α upregulation in hZIP1-knockdown cells. Furthermore, a previous study reported that Zn^{2+} could affect the activity of key enzymes in the tricarboxylic acid cycle and glycolytic pathway, thus improving the cytotoxicity of antitumor drugs (48). HIF-1α often induces the expression of glycolytic enzymes in tumors with abnormally enhanced glycolysis (49). The present study detected the protein expression levels of PDK1, GLUT1 and LDHA after zinc addition, and these three proteins were revealed to be decreased by zinc. The present results suggested that hZIP1 partially suppressed HIF-1α by upregulating FBXO30, and that hZIP1 might directly impair the expression of HIF-1α by enriching intracellular Zn^{2+}. In addition, since Zn^{2+} also upregulated FBXO30 protein expression levels, it is possible that Zn^{2+} may be involved in the ubiquitination process of HIF-1α mediated by FBXO30, which needs further verification.

In conclusion, FBXO30 may be a novel E3 ubiquitin ligase for HIF-1α that is involved in ccRCC progression. We also verified the findings of our previous study that hZIP1 inhibits HIF-1α protein expression (28). In addition, hZIP1 may be upstream of FBXO30, promoting the downregulation of HIF-1α via FBXO30. Furthermore, hZIP1 was revealed to potentially recruit Zn^{2+} to regulate the expression of FBXO30 and HIF-1α, thereby inhibiting glycolysis in ccRCC. However, there were some limitations in the present study. The binding domain in FBXO30 and HIF-1α, and the ubiquitination site remain unknown. In-depth verification is required to determine the effects of hZIP1, Zn^{2+} and FBXO30 on glycolysis at the metabolite level. In addition, the experimental group design needs improvements. There should have been a hZIP1 overexpression group alone tested simultaneously with the hZIP1 overexpression + FBXO30 knockdown group and the FBXO30 knockdown group, to support the conclusion that knockdown of FBXO30 rescued the downregulation of HIF-1α protein expression levels induced by hZIP1. ccRCC is defined as a metabolic disease with highly abnormal glucose metabolism, as well as crosstalk in lipid and amino acid metabolism (50,51). Recently, targeted immunotherapies to alleviate hypoxia and inhibit abnormal metabolic genes have gained attention for application in the complex immune microenvironment in ccRCC (52,53). To a certain extent, the present study verified the probable existence of the hZIP1/Zn^{2+}/FBXO30/HIF-1α axis, which may suppress EMT and glycolysis progression in ccRCC. The present study not only provided novel insights into the occurrence and development of ccRCC, but also identified potential biomarkers or therapeutic targets for the clinical treatment of RCC.

Acknowledgements

Availability of data and materials

The datasets used and/or analyzed during the current study are available from the corresponding author on reasonable request.

Authors' contributions

YY and XD conceived the study and confirmed the authenticity of all the raw data. YY participated in investigation, data curation, visualization and wrote the original draft. ZiL, BL, and ZG were involved in investigation and formal analysis. CP, ZhL and ZZ contributed to the conception and design of the study, and were accountable for all aspects of the work to ensure that questions related to the accuracy or integrity of any part of the work are appropriately investigated and resolved. All authors read and approved the final manuscript.

Ethics approval and consent to participate

The animal experiments performed in the present study were approved by the Ethics Committee of China Medical University (approval no. KT2022527). The experiments using human tissues in the present study were approved by the Research Ethics Committee of China Medical University, and the approval number was [2019]2019-65-3; written informed consent was obtained from all patients.

Patient consent for publication

Not applicable.

Competing interests

The authors declare that they have no competing interests.

References

1. Siegel RL, Miller KD, Fuchs HE and Jemal A: Cancer statistics, 2022. CA Cancer J Clin 72: 7-33, 2022.
2. Xia C, Dong X, Li H, Cao M, Sun D, He S, Yang F, Yan X, Zhang S, Li N and Chen W: Cancer statistics in China and United States, 2022: Profiles, trends, and determinants. Chin Med J (Engl) 135: 584-590, 2022.
3. Hsieh JJ, Purdue MP, Signoretti S, Swanton C, Albiges L, Schmidinger M, Heng DY, Larkin J and Ficarra V: Renal cell carcinoma. Nat Rev Dis Primers 3: 17009, 2017.
4. Cao H, Sun Z, Wu J, Hao C and Wang W: Metastatic clear cell renal cell carcinoma to pancreas and distant organs 24 years after radical nephrectomy: A case report and literature review. Front Surg 9: 894272, 2022.
5. Bai C, Sen P, Hofmann K, Ma L, Goebl M, Harper JW and Elledge SJ: SKP1 connects cell cycle regulators to the ubiquitin proteolysis machinery through a novel motif, the F-box. Cell 86: 263-274, 1996.
6. Nguyen KM and Busino L: The biology of F-box proteins: The SCF family of E3 ubiquitin ligases. Adv Exp Med Biol 1217: 111-122, 2020.
7. Shen W, Zhou Q, Peng C, Li J, Yuan Q, Zhu H, Zhao M, Jiang X, Liu W and Ren C: FBXW7 and the hallmarks of cancer: Underlying mechanisms and prospective strategies. Front Oncol 12: 880077, 2022.
8. Zhu H, Wang X, Zhou X, Lu S, Gu G and Liu C: E3 ubiquitin ligase FBXW7 enhances radiosensitivity of non-small cell lung cancer cells by inhibiting SOX9 regulation of CDKN1A through ubiquitination. Lab Invest 102: 1203-1213, 2022.
9. Nita A, Nishiyama M, Muto Y and Nakayama KI: FBXL12 regulates T-cell differentiation in a cell-autonomous manner. Genes Cells 21: 517-524, 2016.
10. Watanabe K, Yumimoto K and Nakayama KI: FBXO21 mediates the ubiquitylation and proteasomal degradation of EID1. Genes Cells 20: 667-674, 2015.
11. Li D, Xie P, Zhao F, Shu J, Li L, Zhan Y and Zhang L: F-box protein Fbxo3 targets Smurf1 ubiquitin ligase for ubiquitination and degradation. Biochem Biophys Res Commun 458: 941-945, 2015.
12. Tekcham DS, Chen D, Liu Y, Ling T, Zhang Y, Chen H, Wang W, Otkur W, Qi H, Xia T, *et al*: F-box proteins and cancer: An update from functional and regulatory mechanism to therapeutic clinical prospects. Theranostics 10: 4150-4167, 2020.
13. Sartori R, Schirwis E, Blaauw B, Bortolanza S, Zhao J, Enzo E, Stantzou A, Mouisel E, Toniolo L, Ferry A, *et al*: BMP signaling controls muscle mass. Nat Genet 45: 1309-1318, 2013.
14. Jin Y, Yang M, Gao C, Yue W, Liang X, Xie B, Zhu X, Fan S, Li R and Li M: Fbxo30 regulates chromosome segregation of oocyte meiosis. Cell Mol Life Sci 76: 2217-2229, 2019.
15. Cheng X, Pei P, Yu J, Zhang Q, Li D, Xie X, Wu J, Wang S and Zhang T: F-box protein FBXO30 mediates retinoic acid receptor γ ubiquitination and regulates BMP signaling in neural tube defects. Cell Death Dis 10: 551, 2019.
16. Bjerre MT, Strand SH, Nørgaard M, Kristensen H, Rasmussen AK, Mortensen MM, Fredsøe J, Mouritzen P, Ulhøi B, Ørntoft T, *et al*: Aberrant DOCK2, GRASP, HIF3A and PKFP hypermethylation has potential as a prognostic biomarker for prostate cancer. Int J Mol Sci 20: 1173, 2019.
17. Bjerre MT, Nørgaard M, Larsen OH, Jensen SØ, Strand SH, Østergren P, Fode M, Fredsøe J, Ulhøi BP, Mortensen MM, *et al*: Epigenetic analysis of circulating tumor DNA in localized and metastatic prostate cancer: Evaluation of clinical biomarker potential. Cells 9: 1362, 2020.
18. Xiong W, Zeng ZY, Shen SR, Li XL, Li WF, Wang R, Xiong F, Peng C, Zhang QH, Zhou M, *et al*: Studies on the relationship between D6S1581, a high frequency allele imbalance locus, and genetic susceptibility to nasopharyngeal carcinoma. Zhonghua Yi Xue Yi Chuan Xue Za Zhi 20: 311-314, 2003 (In Chinese).
19. Pezzuto A and Carico E: Role of HIF-1 in cancer progression: Novel insights. A review. Curr Mol Med 18: 343-351, 2018.
20. Li JN, Chen PS, Chiu CF, Lyu YJ, Lo C, Tsai LW and Wang MY: TARBP2 suppresses ubiquitin-proteasomal degradation of HIF-1α in breast cancer. Int J Mol Sci 23: 208, 2021.
21. Liu J, Zhang C, Zhao Y, Yue X, Wu H, Huang S, Chen J, Tomsky K, Xie H, Khella CA, *et al*: Parkin targets HIF-1α for ubiquitination and degradation to inhibit breast tumor progression. Nat Commun 8: 1823, 2017.
22. Flügel D, Görlach A and Kietzmann T: GSK-3β regulates cell growth, migration, and angiogenesis via Fbw7 and USP28-dependent degradation of HIF-1α. Blood 119: 1292-1301, 2012.
23. Bowers K and Srai SKS: The trafficking of metal ion transporters of the Zrt- and Irt-like protein family. Traffic 19: 813-822, 2018.
24. Costello LC and Franklin RB: A comprehensive review of the role of zinc in normal prostate function and metabolism; and its implications in prostate cancer. Arch Biochem Biophys 611: 100-112, 2016.
25. Jeong J and Eide DJ: The SLC39 family of zinc transporters. Mol Aspects Med 34: 612-619, 2013.
26. Dineley KE, Votyakova TV and Reynolds IJ: Zinc inhibition of cellular energy production: Implications for mitochondria and neurodegeneration. J Neurochem 85: 563-570, 2003.
27. Dong X, Kong C, Zhang Z, Liu X, Zhan B, Chen Z and Shi D: hZIP1 that is down-regulated in clear cell renal cell carcinoma is negatively associated with the malignant potential of the tumor. Urol Oncol 32: 885-892, 2014.
28. Zhan B, Dong X, Yuan Y, Gong Z and Li B: hZIP1 inhibits progression of clear cell renal cell carcinoma by suppressing NF-kB/HIF-1α pathway. Front Oncol 11: 759818, 2021.
29. Delahunt B, Eble JN, Egevad L and Samaratunga H: Grading of renal cell carcinoma. Histopathology 74: 4-17, 2019.
30. Livak KJ and Schmittgen TD: Analysis of relative gene expression data using real-time quantitative PCR and the 2(-Delta Delta C(T)) method. Methods 25: 402-408, 2001.
31. Ma X, Li C, Sun L, Huang D, Li T, He X, Wu G, Yang Z, Zhong X, Song L, *et al*: Lin28/let-7 axis regulates aerobic glycolysis and cancer progression via PDK1. Nat Commun 5: 5212, 2014.
32. Park JS, Lee ME, Kim SH, Jang WS and Ham WS: Development of a highly pulmonary metastatic orthotopic renal cell carcinoma murine model. Biol Open 10: bio058566, 2021.
33. Schödel J, Grampp S, Maher ER, Moch H, Ratcliffe PJ, Russo P and Mole DR: Hypoxia, hypoxia-inducible transcription factors, and renal cancer. Eur Urol 69: 646-657, 2016. Wilson WR and Hay MP: Targeting hypoxia in cancer therapy. Nat Rev Cancer 11: 393-410, 2011.
34. Wigerup C, Påhlman S and Bexell D: Therapeutic targeting of hypoxia and hypoxia-inducible factors in cancer. Pharmacol Ther 164: 152-169, 2016.
35. Choi WSW, Boland J and Lin J: Hypoxia-inducible factor-2α as a novel target in renal cell carcinoma. J Kidney Cancer VHL 8: 1-7, 2021.
36. Rashid M, Zadeh LR, Baradaran B, Molavi O, Ghesmati Z, Sabzichi M and Ramezani F: Up-down regulation of HIF-1α in cancer progression. Gene 798: 145796, 2021.
37. Doonachar A, Gallo MD, Doukas D, Pasricha R, Lantsberg I and Schoenfeld AR: Differential effects of HIF-α isoforms on apoptosis in renal carcinoma cell lines. Cancer Cell Int 15: 23, 2015.
38. Hoefflin R, Harlander S, Schäfer S, Metzger P, Kuo F, Schönenberger D, Adlesic M, Peighambari A, Seidel P, Chen CY, *et al*: HIF-1α and HIF-2α differently regulate tumour development and inflammation of clear cell renal cell carcinoma in mice. Nat Commun 11: 4111, 2020.
39. Chen N, Kong X, Zhao S and Xiaofeng W: Post-translational modification of baculovirus-encoded proteins. Virus Res 279: 197865, 2020.
40. Morishita Y, Ookawara S, Hirahara I, Muto S and Nagata D: HIF-1α mediates hypoxia-induced epithelial-mesenchymal transition in peritoneal mesothelial cells. Ren Fail 38: 282-289, 2016.
41. Das B, Tsuchida R, Malkin D, Koren G, Baruchel S and Yeger H: Hypoxia enhances tumor stemness by increasing the invasive and tumorigenic side population fraction. Stem Cells 26: 1818-1830, 2008.
42. Ide T, Kitajima Y, Miyoshi A, Ohtsuka T, Mitsuno M, Ohtaka K, Koga Y and Miyazaki K: Tumor-stromal cell interaction under hypoxia increases the invasiveness of pancreatic cancer cells through the hepatocyte growth factor/c-Met pathway. Int J Cancer 119: 2750-2759, 2006.
43. Skrajnowska D and Bobrowska-Korczak B: Role of zinc in immune system and anti-cancer defense mechanisms. Nutrients 11: 2273, 2019.
44. To PK, Do MH, Cho JH and Jung C: Growth modulatory role of zinc in prostate cancer and application to cancer therapeutics. Int J Mol Sci 21: 2991, 2020.

45. Gelbard A: Zinc in cancer therapy revisited. Isr Med Assoc J 24: 258-262, 2022.
46. Liu L, Hou Y, Hu J, Zhou L, Chen K, Yang X and Song Z: SLC39A8/zinc suppresses the progression of clear cell renal cell carcinoma. Front Oncol 11: 651921, 2021.
47. Nardinocchi L, Pantisano V, Puca R, Porru M, Aiello A, Grasselli A, Leonetti C, Safran M, Rechavi G, Givol D, *et al*: Zinc downregulates HIF-1α and inhibits its activity in tumor cells in vitro and in vivo. PLoS One 5: e15048, 2010.
48. Olechnowicz J, Tinkov A, Skalny A and Suliburska J: Zinc status is associated with inflammation, oxidative stress, lipid, and glucose metabolism. J Physiol Sci 68: 19-31, 2018.
49. Kierans SJ and Taylor CT: Regulation of glycolysis by the hypoxia-inducible factor (HIF): Implications for cellular physiology. J Physiol 599: 23-37, 2021.
50. Chakraborty S, Balan M, Sabarwal A, Choueiri TK and Pal S: Metabolic reprogramming in renal cancer: Events of a metabolic disease. Biochim Biophys Acta Rev Cancer 1876: 188559, 2021.
51. Wise DR and Thompson CB: Glutamine addiction: A new therapeutic target in cancer. Trends Biochem Sci 35: 427-433, 2010.
52. Lai Y, Tang F, Huang Y, He C, Chen C, Zhao J, Wu W and He Z: The tumour microenvironment and metabolism in renal cell carcinoma targeted or immune therapy. J Cell Physiol 236: 1616-1627, 2021.
53. Li F, Aljahdali IAM, Zhang R, Nastiuk KL, Krolewski JJ and Ling X: Kidney cancer biomarkers and targets for therapeutics: Survivin (BIRC5), XIAP, MCL-1, HIF1α, HIF2α, NRF2, MDM2, MDM4, p53, KRAS and AKT in renal cell carcinoma. J Exp Clin Cancer Res 40: 254, 2021.